

# ASPECTS OF STRUCTURAL LANDSCAPE OF HUMAN ISLET AMYLOID POLYPEPTIDE

Jianfeng He,<sup>1,\*</sup> Jin Dai,<sup>1,†</sup> Jing Li,<sup>2,‡</sup> Xubiao Peng,<sup>3,§</sup> and Antti J. Niemi<sup>4,3,1,¶</sup>

<sup>1</sup>*School of Physics, Beijing Institute of Technology, Beijing 100081, P.R. China*

<sup>2</sup>*Institute of Biopharmaceutical Research,*

*Yangtze River Pharmaceutical Group*

*Beijing Haiyan Pharmaceutical Co., Ltd, Beijing 102206, China*

<sup>3</sup>*Department of Physics and Astronomy, Uppsala University,*

*P.O. Box 803, S-75108, Uppsala, Sweden*

<sup>4</sup>*Laboratoire de Mathématiques et Physique Théorique CNRS UMR 6083,*

*Fédération Denis Poisson, Université de Tours,*

*Parc de Grandmont, F37200, Tours, France*

## Abstract

The human islet amyloid polypeptide (hIAPP) co-operates with insulin to maintain glycemic balance. It also constitutes the amyloid plaques that aggregate in the pancreas of type-II diabetic patients. We have performed extensive *in silico* investigations to analyse the structural landscape of monomeric hIAPP, which is presumed to be intrinsically disordered. For this we construct from first principles a highly predictive energy function that describes a monomeric hIAPP observed in a NMR experiment, as a local energy minimum. We subject our theoretical model of hIAPP to repeated heating and cooling simulations, back and forth between a high temperature regime where the conformation resembles a random walker and a low temperature limit where no thermal motions prevail. We find that the final low temperature conformations display a high level of degeneracy, in a manner which is fully in line with the presumed intrinsically disordered character of hIAPP. In particular, we identify an isolated family of  $\alpha$ -helical conformations that *might* cause the transition to amyloidosis, by nucleation.

---

\*Electronic address: [hjf@bit.edu.cn](mailto:hjf@bit.edu.cn)

†Electronic address: [daijing491@gmail.com](mailto:daijing491@gmail.com)

‡Electronic address: [jinglichina@139.com](mailto:jinglichina@139.com)

§Electronic address: [xubiaopeng@gmail.com](mailto:xubiaopeng@gmail.com)

¶Electronic address: [Antti.Niemi@physics.uu.se](mailto:Antti.Niemi@physics.uu.se); URL: <http://www.folding-protein.org>

## I. INTRODUCTION

The human islet amyloid polypeptide (hIAPP), also known as amylin, is a widely studied 37 amino acid polypeptide hormone.<sup>1-3</sup> hIAPP is processed in pancreatic  $\beta$ -cells, by a protease cleavage in combination of post-translational modifications. Its secretion responds to meals, and the peptide co-operates with insulin to regulate blood glucose levels. But hIAPP can also aggregate into pancreatic amyloid deposits. The formation and buildup of amyloid fibrils correlates strongly with the depletion of islet  $\beta$ -cells. The hIAPP amyloidosis is present in over 90 per cent of the type-II diabetic patients<sup>4-7</sup> and the deposits are considered the hallmark of the disease in progression. Early studies<sup>8,9</sup> suggested that the fibrils themselves could be the toxic agents that cause cell death. However, recently it has been found that the formation of amyloid plaques is most likely a sufficient and not a necessary condition for the disruption of  $\beta$ -cells<sup>10,11</sup>. It appears that the cause for the islet  $\beta$ -cell depletion is somewhere upstream from the formation and buildup of amyloid fibrils. The initial step seems to be an intracellular process that takes place in endoplasmic reticulum, golgi or secretory granules<sup>1-3</sup>.

Experimentally, the structure of hIAPP amyloid fibrils has been studied extensively. See for example<sup>12-32</sup>. We note that the fibrils consist of an ordered parallel arrangement of hIAPP monomers, with the cross- $\beta$  spine displaying a zipper-like packing. Atomic level investigation of the cross- $\beta$  spine reveals that the segment which consists of residues 21-27 (NNFGAIL) forms a turn, that joins sheets which are made up of the residues 28-33 (SSTNVG), into a classic steric zipper<sup>21</sup>. According to<sup>27,28</sup> the fibril formation proceeds by nucleation, so that one hIAPP molecule first assumes a hairpin structure with two  $\beta$ -strands linked by a loop. This is followed by a piling-up of monomers. However, the structure of a full-length *monomeric* hIAPP, and in particular the intra-cellular conformational pathways that lead to the  $\beta$ -hairpin nucleation causing conformation, remain unknown<sup>3</sup>. The sole crystallographic structure with Protein Data Bank (PDB) access code 3G7V<sup>22</sup> describes hIAPP fused with a maltose-binding protein. Two solution NMR structures are available in PDB. The PDB access codes are 2KB8<sup>23</sup> and 2L86<sup>25</sup>. These three presently available PDB structures are all very different from each other. Indeed, an isolated hIAPP is presumed to be an example of a dynamical, intrinsically disordered protein<sup>33</sup>. When biologically active, such proteins are often presumed to be in a perpetual motion, fulfilling their biological function by constantly

varying their shape. Thus these proteins lack an ordered folded conformation that could be studied *e.g.* by conventional x-ray crystallography approaches. Moreover, detergents such as SDS micelles that are introduced as stabilising agents in solution NMR experiments, may lead to structural distortions.

The detailed atomic level structure of hIAPP conformations could in principle be extracted using molecular dynamics simulations. Indeed, both all-atom and coarse-grained molecular dynamics force fields are being employed to try and understand *in silico* the structure of hAIPP, both in fibrils and in isolation; see *e.g.*<sup>30,34-40</sup>, and we refer to<sup>41</sup> for a recent detailed review. However, in particular when explicit water is introduced in the simulations, the computational task becomes staggering: The special purpose molecular dynamics machine *Anton*<sup>42,43</sup> is capable of describing *in vitro/in vivo* trajectories up to around a microsecond per a day *in silico*. At the same time, amyloid aggregation takes hours, even days. Thus the quality of present MD based investigations of hIAPP depends largely on our ability to determine the initial conformation in the simulations<sup>41</sup>.

In the present article we investigate computationally the structural properties of the hIAPP segment, that consists of the residues 9-37 where several studies have either observed or predicted that the amyloid fibril formation starts<sup>1-3,19,44-57</sup>. The physical properties of the short N-terminal segment that comprises the residues 1-8 is not addressed here. Its structure is more involved, due to the disulfide bond that forms between the cysteines which are located at the residues 2 and 7<sup>58,59</sup>. Moreover, it remains to be understood what is the rôle of the residues 1-8 in hIAPP aggregation<sup>60</sup>. These residues appear to have a tendency towards forming long and stable non- $\beta$ -sheet fibers in solution, under the same conditions in which hIAPP aggregates into amyloid fibers. We note that a peptide, which consists only of the sites 17-37 of hIAPP, has also been identified both in human pancreas and plasma<sup>61</sup>. But its biological rôle remains to be clarified.

Our approach is based on an universal energy function<sup>62,63</sup>; see<sup>64</sup> for a detailed description. This approach builds on the powerful techniques of universality and renormalisation groups<sup>65-68</sup> in combination with the notion of local gauge symmetry. Instead of a short time step expansion on which the MD approaches are based, we expand in terms of variables that have slow spatial variations; in the continuum limit this becomes an expansion in terms of derivatives. As such our approach should provide complementary information to MD approaches. In particular, since the notion of a short time step is avoided we can in principle

cover very long time scales.

We note that the technique of universality was originally introduced to describe phase transitions and critical phenomena, while the method of renormalization group originates from high energy physics. Both have subsequently found numerous applications for example in dynamical systems and chaos, in statistical polymer research, and in analysis of nonlinear ordinary and partial differential equations.

We use the NMR structure 2L86<sup>25</sup> as a decoy to train the energy function. The 2L86 is measured at pH of 7.4 *i.e.* around the pH value in the extracellular domain, where the actual amyloid deposit aggregation takes place. We follow<sup>69-77</sup> to construct a static multi-kink configuration as an extremum of the energy function, so that it accurately describes the hIAPP structure in 2L86.

The 2L86 is a composite of hIAPP with SDS micelles. It is often thought that SDS micelles could model the effects of a cell membrane. Thus our simulations correspond to the following biological set-up: We consider the structural evolution of an isolated hIAPP in the extracellular domain where it has the initial shape of 2L86, and is in an initial interaction with the cell membrane. We study the evolution of the hIAPP conformation as it departs the cell membrane. For this we inquire whether there are local energy minima, with a lower energy than that of the multi-kink which models 2L86.

We subject the multi-kink to a series of heating and cooling simulations<sup>73-75</sup>. During the heating, we increase the temperature until we detect a structural change in the multi-kink, so that the configuration behaves like a random walker, and we fully thermalise the configuration at the random walk temperature. The heating enables the multi-kink to cross over the energy barriers which surround the initial 2L86 conformation, in search of lower energy states. We then reduce the ambient temperature, to cool down the configuration to *very* low temperature values until it freezes into a conformation where no thermal motion prevails. According to Anfinsen<sup>78</sup>, upon cooling the protein should assume a fold, which is a local minimum of the low temperature thermodynamic (Helmholtz) free energy. More specifically, in the case of a protein with an ordered native fold, the heating and cooling cycle should produce a highly localized statistical distribution of structurally closely related conformational substates. When taken together, this ensemble constitutes the folded native state at low temperatures<sup>79</sup>. In the case of the energy function introduced in<sup>69-72</sup> this has been shown to occur *in silico*, with a number of proteins that are known to possess an

ordered native fold<sup>73–75</sup>.

But for a protein which is intrinsically disordered, instead we expect that the low temperature limit produces a *scattered* statistical distribution of structurally disparate but energetically comparable ensembles of conformational substates. Moreover, these different substates should be separated from each other by relatively low energy barriers. We propose that the unstructured, disordered character of the protein is a consequence of a motion around this landscape: The protein swings and sways back and forth, quite freely, over the low energy barriers that separate the various energetically degenerate but structurally disparate conformations. We now proceed to show that in the case of hIAPP, heating and cooling procedure yields exactly this kind of structurally scattered ensembles of conformations.

## II. METHODS

### A. C $\alpha$ backbone

Let  $\mathbf{r}_i$  be the skeletal C $\alpha$  coordinates of a protein, with  $i = 1, \dots, N$ . Introduce the unit tangent vectors  $\mathbf{t}_i$ , unit binormal vectors  $\mathbf{b}_i$ , and unit normal vectors  $\mathbf{n}_i$

$$\mathbf{t}_i = \frac{\mathbf{r}_{i+1} - \mathbf{r}_i}{|\mathbf{r}_{i+1} - \mathbf{r}_i|} \quad \& \quad \mathbf{b}_i = \frac{\mathbf{t}_{i-1} \times \mathbf{t}_i}{|\mathbf{t}_{i-1} \times \mathbf{t}_i|} \quad \& \quad \mathbf{n}_i = \mathbf{b}_i \times \mathbf{t}_i \quad (1)$$

The orthonormal triplet  $(\mathbf{n}_i, \mathbf{b}_i, \mathbf{t}_i)$  determines the discrete Frenet frame<sup>80</sup> at the position  $\mathbf{r}_i$  of the backbone; see figure 1. The C $\alpha$  backbone bond and torsion angles, shown in Figure 2, are computed as follows

$$\kappa_i \equiv \kappa_{i+1,i} = \arccos(\mathbf{t}_{i+1} \cdot \mathbf{t}_i) \quad (2)$$

$$\tau_i \equiv \tau_{i+1,i} = \text{sign}\{\mathbf{b}_i \times \mathbf{b}_{i+1} \cdot \mathbf{t}_i\} \cdot \arccos(\mathbf{b}_{i+1} \cdot \mathbf{b}_i) \quad (3)$$

Alternatively, if these angles are all known, we can use the discrete Frenet equation<sup>80</sup>

$$\begin{pmatrix} \mathbf{n} \\ \mathbf{b} \\ \mathbf{t} \end{pmatrix}_{i+1} = \begin{pmatrix} \cos \kappa \cos \tau & \cos \kappa \sin \tau & -\sin \kappa \\ -\sin \tau & \cos \tau & 0 \\ \sin \kappa \cos \tau & \sin \kappa \sin \tau & \cos \kappa \end{pmatrix}_{i+1,i} \begin{pmatrix} \mathbf{n} \\ \mathbf{b} \\ \mathbf{t} \end{pmatrix}_i \quad (4)$$

to construct all the frames along the entire C $\alpha$  backbone chain. Once we have constructed all the frames, we obtain the backbone coordinates from

$$\mathbf{r}_k = \sum_{i=0}^{k-1} |\mathbf{r}_{i+1} - \mathbf{r}_i| \cdot \mathbf{t}_i \quad (5)$$

Fig 1  
Fig 2

In (5) we may set  $\mathbf{r}_0 = 0$ , and we may choose  $\mathbf{t}_0$  to point along the positive  $z$ -axis. With the exception of *cis*-proline which is rare, we may take the distance between any two neighboring  $C\alpha$  atoms to have a constant value

$$|\mathbf{r}_{i+1} - \mathbf{r}_i| \approx 3.8 \text{ \AA}$$

This approximation is valid at time scales which are much longer than the characteristic time scale of covalent bond vibration; here we are interested in the limit of such long time scales. For any two  $C\alpha$  atoms that are not next to each other along the backbone chain, the PDB structures are consistent with the steric constraint

$$|\mathbf{r}_i - \mathbf{r}_k| > 3.8 \text{ \AA} \quad \text{for } |i - k| \geq 2 \quad \text{steric} \quad (6)$$

The positions of the backbone N, C, O and H atoms and the side-chain  $C\beta$  atoms can be determined quite precisely in terms of the  $C\alpha$  coordinates<sup>81-87</sup>. Similarly, several higher level side-chain atoms assume rotamer positions with respect to the  $C\alpha$  backbone.<sup>81-87</sup> The  $C\alpha$  backbone is also widely exploited in structural classification schemes such as SCOP<sup>88</sup> and CATH<sup>89</sup>, in homology modeling<sup>90</sup>, in *de novo* approaches<sup>91</sup>, and in the development of coarse grained energy functions for folding prediction<sup>92</sup>. The goal of the so called  $C\alpha$ -trace problem<sup>93-97</sup> is to construct an accurate all-atom model of the natively folded protein from the positions of the central  $C\alpha$  atoms. Both knowledge-based approaches such as MAXSPROUT<sup>93</sup> and *de novo* methods including PULCHRA<sup>95</sup> and SCWRL<sup>97</sup> address the  $C\alpha$ -trace problem. It has been shown that the virtual  $C\alpha$  backbone bond ( $\kappa_i$ ) and torsion ( $\tau_i$ ) angles are sufficient to determine the structure of any protein in Protein Data Bank, with very high precision<sup>98</sup>. Thus, the  $C\alpha$  coordinates form an attractive set of variables to try and approximate the structure and dynamics of proteins.

## B. Universal energy function

A folded protein minimises locally the thermodynamical Helmholtz free energy

$$F = U - TS \quad \text{Helm} \quad (7)$$

where  $U$  is the internal energy,  $S$  is the entropy, and  $T$  is the temperature. The free energy is a function of all the inter-atomic distances

$$F = F(r_{\alpha\beta}) ; \quad r_{\alpha\beta} = |\mathbf{r}_\alpha - \mathbf{r}_\beta| \quad \text{intat} \quad (8)$$

where index  $\alpha, \beta, \dots$  extends over all the atoms in the protein system. In the case of slowly varying deformations, we may follow the general *universality* arguments in<sup>65–68</sup>. These arguments instruct us to adopt the C $\alpha$  backbone bond and torsion angles as the structural order parameters to characterise the protein conformation in the vicinity of the free energy minimum,

$$r_{\alpha\beta} = r_{\alpha\beta}(\kappa_i, \tau_i)$$

Accordingly, when deformations around a minimum energy configuration remain slow and small we may expand the free energy in terms of the C $\alpha$  bond and torsion angles. In<sup>62,63,69–75</sup> it has been shown that in the limit of slowly varying variables, the free energy  $F$  expands as follows:

$$F = - \sum_{i=1}^{N-1} 2 \kappa_{i+1} \kappa_i + \sum_{i=1}^N \left\{ 2\kappa_i^2 + \lambda (\kappa_i^2 - m^2)^2 + \frac{q}{2} \kappa_i^2 \tau_i^2 - p \tau_i + \frac{r}{2} \tau_i^2 \right\} + \dots \quad (9)$$

Here  $\lambda$ ,  $q$ ,  $p$ ,  $r$ , and  $m$  depend on the atomic level physical properties and the chemical microstructure of the protein and its environment, and in principle these parameters can be computed from this knowledge. We note the following: The free energy (9) is a variant of the energy function of the discrete nonlinear Schrödinger equation (DNLS)<sup>99,100</sup>: The first sum together with the three first terms in the second sum is the energy of the standard DNLS equation, in terms of the discretized Hasimoto variable<sup>101</sup>. The fourth term ( $p$ ) is the conserved "helicity", it is responsible for the chirality of the C $\alpha$  backbone. The last ( $r$ ) term is the Proca mass.

*A priori*, the fundamental range of the bond angle  $\kappa_i$  is  $[0, \pi]$ . For the torsion angle the fundamental range is  $\tau_i \in [-\pi, \pi)$ . Consequently  $(\kappa_i, \tau_i)$  can be identified with the canonical latitude and longitude angles on the surface of a sphere. In the sequel we find it useful to extend the fundamental range of  $\kappa_i$  into  $[-\pi, \pi]$  but with no change in the fundamental range of  $\tau_i$ . We compensate for this two-fold covering of the sphere, by the following discrete  $\mathbb{Z}_2$  symmetry<sup>80</sup>

$$\begin{aligned} \kappa_l &\rightarrow -\kappa_l && \text{for all } l \geq i \\ \tau_i &\rightarrow \tau_i - \pi \end{aligned} \quad \text{dsgau} \quad (10)$$

Finally, we note that regular protein secondary structures correspond to constant values of  $(\kappa_i, \tau_i)$ . For example standard  $\alpha$ -helix and  $\beta$ -strand are

$$\alpha\text{-helix} : \begin{cases} \kappa \approx \frac{\pi}{2} \\ \tau \approx 1 \end{cases} \quad \& \quad \beta\text{-strand} : \begin{cases} \kappa \approx 1 \\ \tau \approx \pi \end{cases} \quad \text{bc2} \quad (11)$$



Similarly, all the other regular secondary structures such as 3/10 helices, left-handed helices *etc.* are structures with definite constant values of  $\kappa_i$  and  $\tau_i$ . A loop can be defined to be any  $(\kappa_i, \tau_i)$  configuration that interpolates between the regular structures. Along a loop the values of  $(\kappa_i, \tau_i)$  are variable, from site to site.

### C. Training the energy

All the parameters in (9) are in principle computable from the atomic level knowledge of the protein, the solvent, and the environmental characteristics including temperature, pressure, acidity and so forth. These parameters can also be estimated from molecular dynamics simulations, or by comparison with experimentally known structures. Here we use the experimental structure: We consider the residues 9-37 in the hIAPP polypeptide with Protein Data Bank (PDB) code 2L86. We train the energy function (9) to model this configuration.

Fig 3 The PDB entry 2L86 consists of 20 NMR different configurations. In Figure 3 we show an interlaced summary of these configurations. Note the presence of substantial fluctuations in the residues 1-8 of the N-terminal. The residues 9-37 form a much more stable structure; as can be seen in Figure 3 the variations between the NMR structures are minor, over the sites 9-37. Any of the 20 different NMR structures could be utilized, to train the energy function (9). A structure obtained *e.g.* by averaging the NMR structures could also be used. The differences between these choices are minor, and for concreteness we use here the first NMR structure in the PDB entry 2L86. We determine the parameters so that the extremum of (9) coincides with the profile of the 2L86: A variation of (9) with respect to  $\tau_i$  gives

$$\begin{aligned} \frac{\partial F}{\partial \tau_i} &= d\kappa_i^2 \tau_i + c\tau_i - a - b\kappa_i^2 = 0 \\ \Rightarrow \tau_i[\kappa] &= \frac{a + b\kappa_i^2}{c + d\kappa_i^2} \end{aligned} \quad (12)$$

We evaluate the derivative of the energy with respect to  $\kappa_i$ . We substitute  $\tau_i[\kappa]$  from (12) into the ensuing equation. We arrive at the following modified version of the DNLS equation

$$\kappa_{i+1} - 2\kappa_i + \kappa_{i-1} = U'[\kappa_i]\kappa_i \equiv \frac{dU[\kappa]}{d\kappa_i^2} \kappa_i \quad (i = 1, \dots, N) \quad (13)$$

(with  $\kappa_0 = \kappa_{N+1} = 0$ ) where

$$U[\kappa] = -\frac{1}{d} (ad - bc)^2 \frac{1}{c + d\kappa^2} - \frac{1}{2d} (b^2 + 4qdm^2) \kappa^2 + q\kappa^4$$

This equation coincides with the stationary points of the energy function

$$H = -2 \sum_{i=1}^{N-1} \kappa_{i+1} \kappa_i + \sum_{i=1}^N \{2\kappa_i^2 + U[\kappa_i]\}$$

For proper parameter values the equation (13) supports a kink solution. The explicit form of the kink, in terms of elementary functions, is not known. But an approximation can be constructed numerically *e.g.* by using the iterative procedure described in reference 70. We use the program package *ProPro* which is based on this iterative procedure, and described in

$$\text{http} : // \text{www.folding} - \text{protein.org} \tag{14}$$

to construct the parameters.

#### D. Heating and cooling

We study the energy landscape of the hIAPP by subjecting the energy function (9) that we have trained with the NMR structure 2L86 of hIAPP, to extensive heating and cooling simulations. It has been argued that in the case of simple proteins, the folding dynamics follows Arrhenius law. On the other hand, a simple spin system with dynamics determined by Glauber protocol<sup>102-105</sup> is also subject to Arrhenius law. This proposes that we try and describe out-of-thermal-equilibrium dynamics of hIAPP using a combination of (9) with Glauber protocol. The transition probability  $\mathcal{P}(i \rightarrow j)$  between any two states  $i$  and  $j$  is evaluated from

$$\mathcal{P} = \frac{x}{1+x} \quad \text{with} \quad x = \exp\left\{-\frac{\Delta E}{kT}\right\} \tag{15}$$

The energy difference  $\Delta E$  between the two states is computed from the free energy (9). We take all parameters in (9) to be temperature independent. As a consequence the temperature factor  $kT$  is not directly related to the physical temperature factor  $k_B t$ . But it can be related to the physical temperature by the renormalization procedure detailed in<sup>74</sup>. Here we are interested in the low temperature limit energy landscape, thus the renormalization has no practical significance.

A full heating and cooling cycle involves  $5 \times 10^7$  Monte Carlo steps, which we have found to be adequate. The cycle starts with a very low temperature value. After a preliminary thermalization of the initial configuration during  $5 \times 10^6$  steps in the low temperature regime,

we proceed to increase the temperature during  $10^7$  MC steps. This is followed by a high temperature thermalization during  $2 \times 10^7$  MC steps, after which we cool the system down during  $10^7$  MC steps to the initial low temperature value where we then allow it to become fully thermalized. We have tested a number of different alternatives but *e.g.* an increase in the number of steps does not have any observable effect on the results.

Glauber dynamics is known to provide a quasi-realistic temporal evolution of a non-equilibrium process where the heating and cooling proceeds slowly, with respect to the atomic scale. Thus we trust that in combination with our universal energy function, the evolution we obtain with (15) describes the universal statistical aspects of hIAPP trajectories over biologically relevant distance and time scales.

### III. RESULTS

#### A. The three-kink solution

In Table I we list the parameter values, that find by training the energy function (9) to describe 2L86. Note that there are only 21 parameters, while there are a total of 28 amino acids in 2L86 *i.e.* there are *less* parameters than there are amino-acids ! This implies that the physical principles from which the energy function (9) derives, can be subjected to *very* stringent experimental scrutiny. Note also that in those terms of (9) that engage the torsion angles, the numerical parameter values are consistently much smaller than in those terms that involve only the bond angles. This is in line with the observation, that in proteins the torsion angles *i.e.* dihedrals are usually quite flexible while the bond angles are relatively stiff.

Table I

Fig 4

In Figure 4 a) we show the spectrum of bond and torsion angles for the first NMR structure of 2L86, with the convention that the bond angle takes values between  $\kappa \in [0, \pi]$ . In Figure 4 b) we have introduced the  $\mathbb{Z}_2$  symmetry (10) to disclose that there are three individual kinks along the backbone. The first kink from the N-terminal is centered at the site 17. The third kink is centered at the site 27. Both of these two kinks correspond to clearly visible loops in the three dimensional structure, seen in Figure 3. The second kink, centered at site 23, is much less palpable in the three dimensional NMR structure. This kink appears more like a bend in an  $\alpha$ -helical structure, extending from the first kink to the

third kink. This  $\mathbb{Z}_2$  transformed  $(\kappa, \tau)$  profile in Figure 4 b) is the background in (9).

Fig 5 In Figure 5 we compare the bond and torsion angle spectrum of our three-kink solution with the first NMR structure of 2L86; the solution is obtained by numerically solving the equations (13), (12) using the program *ProPro* described at (14). Clearly, the quality of our three-kink solution is very good, at the level of the bond and torsion angles.

Fig 6 Figure 6 shows our three-kink solution, interlaced with the first NMR structure of 2L86. The RMSD distance between the experimental structure and the three-kink configuration is 1.17 Å. This is somewhat large, when compared to the multi-kink structures that have been presented in<sup>73-75</sup>; typically a multi-kink configuration describes a high resolution crystallographic structure with a RMSD precision much below 1.0 Å. But the resolution of the present experimental NMR structure is not that good, and this is reflected by the somewhat lower quality of the three-kink solution, in comparison to the case of high resolution crystallographic structures.

Fig 7 Figure 7 compares the residue-wise  $C\alpha$  distances, between the 20 different NMR structures in the PDB entry 2L86, and our three-kink solution. For those residues that precede the bend-like second kink which is centered at site 23, the distance between the experimental structures and the numerically constructed solution is relatively small. There is a quantitative change in the precision of the three-kink solution, that takes place after site 23: The distance between the experimental structures and the three-kink solution increases after this residue. We propose that this change is due to the SDS micelles, used in the experimental set-up to stabilize hIAPP/2L86: Sodium dodecyl sulfate (SDS) is widely used as a detergent, to enable NMR structure determination in the case of proteins with high hydrophobicity<sup>106-109</sup>. The mechanism of SDS-protein interaction is not yet fully understood. But it is known that the hydrophobic tails of SDS molecules interact in particular with the hydrophobic core of a protein. These interactions are known to disrupt the native structure to the effect, that the protein displays an increase in its  $\alpha$ -helical posture. These additional  $\alpha$ -helical structures tend to be surrounded by SDS micelles.

The residue site 23 of hIAPP is the highly hydrophobic phenylalanine. It is followed by the very flexible glycine at site 24. Thus, the apparently abnormal bend which is located at the site 23 and affects the quality of our three-kink configuration, could be due to an interaction between the phenylalanine and the surrounding SDS micelles. We note that a high sensitivity of the hIAPP conformation to the phenylalanine at site 23 has been recorded

in several studies<sup>110–112</sup>.

An analysis of 2L86 structure using MOLPROBITY<sup>113</sup> suggests a propensity towards poor rotamers between the sites 23-36, *i.e.* the region where the quality of our three-kink solution decreases.

A comparison with the statistically determined radius of gyration relation<sup>114</sup>

$$R_g \approx 2.29 \cdot N^{0.37} \tag{16}$$

where  $N$  is the number of residues, reveals that for 2L86 the value of  $R_g \approx 9.2$  (over residues  $N = 9, \dots, 36$ ) is somewhat high. According to (16), we expect a value close to  $R_g \approx 7.9$  (with  $N = 28$  residues): The structure of 2L86 should be more compact.

We conclude that most likely the SDS-hIAPP interaction has deformed a loop which, in the absence of micelles, should be located in the vicinity of the residue number 23. Probably, the interaction with micelles has converted this loop into a structure resembling a bend in an  $\alpha$ -helix. This interaction between hIAPP and SDS interferes with our construction of the three-kink configuration, adversely affecting its precision.

**B. Heating and cooling of hIAPP**

Fig 8 The Figures 8 describe the evolution of the three-kink configuration during repeated heating and cooling. The Figure 8 (top) shows the evolution of the radius of gyration, and the Figure 8 (bottom) shows the RMSD distance to the PDB structure 2L86. Both the average value and the one standard deviation from the average value, are shown. During the cooling period we observe only one transition, in both the radius of gyration and the RMSD. Thus, we are confident that at high temperatures we are in the random walk regime<sup>73–75</sup>. The profile of each curve in Figure 8 shows that the structures are fully thermalized, both in the high temperature and in the low temperature regimes.

We observe that the average final value of the radius of gyration  $R_g \approx 7.8$  is an excellent match with the prediction obtained from (16). The final configurations are quite different from the initial configuration: The RMSD distance between the initial configuration and the average final configuration is around 4.8 Å.

Figure 9 shows results for a representative simulation with ~1.500 complete heating and cooling cycles; an increase in the number of cycles does not have a qualitative effect. The

Figure shows the distribution of the final conformations, grouped according to their radius of gyration versus end-to-end distance. The final conformations form clusters, and we have identified the six major clusters that we observe in our simulations. By construction, the clusters correspond to local extrema of the energy function we have constructed to model 2L86. Five of the clusters, denoted 2-6 in the Figure, have an apparent spread, there is a flat direction in the energy around its extremum. The clusters 3 and 5 are also somewhat more scattered than the clusters 2, 4 and 6. Finally, the cluster number 1 is a localized one. Note that the initial conformation, marked with red triangle in the Figure 9, does not appear among the final configurations. It is apparently an unstable extremum of the energy.

Fig 9

In Figure 10 we display the average conformations in each of the six clusters, interlaced with each other and the initial 2L86 configuration. In this Figure, the first two C $\alpha$  atoms from the N-terminus are made to coincide. We have maximized the alignment of the subsequent C $\alpha$  atoms, to the extent it is possible. The Figure reveals the presence of substantial conformational difference between the clusters.

Fig 10

In Figures 11 we compare the individual clusters shown in Figure 10, with the initial 2L86 configuration (in blue). In each of these Figures, we show ten representative entries in each of the clusters (in red), to visualize the extent of conformational fluctuations within each cluster. We observe that the conformational spread within each of the six clusters is not very large.

Fig 11

### C. Side-chain atoms

We have reconstructed the full atom configurations for every structure shown in Figures 10, 11 using both PULCHRA<sup>95</sup> and SCWRL<sup>97</sup>. We have excluded *all* configurations where *any* pair of heavy atoms either in the backbone or in the side-chain, that are *not* covalently bonded to each other, have a mutual distance less than 1.2 Å. In this manner we have obtained the distributions shown in Figures 12, for PULCHRA and SCWRL respectively.

We observe that qualitatively, the differences between Figures 9 and 12 are minor; the majority of the structures that appear in Figure 9 are also consistent with the side-chain assignments given by both PULCHRA and SCWRL, when combined with the requirement that any pair of atoms must have a minimum distance of 1.2 Å unless they are covalently

Fig 12

bonded; for the  $C\alpha$  atoms we have the bound (6) during our entire simulations.

Finally, in Figures 13 and 14 we display the hydrophobic side-chains, for the average configurations in each of the six clusters shown in Figure 9. We observe that the hydrophobic side-chains are by and large exposed to the solvent. A notable exception is the pair L-16 and V-32 in cluster 1 which are *very* proximal to each other. Note that I-26 is also close-by. Since V and L are known to be mutually attractive<sup>115</sup>, we conclude that the proximity of this pair enhances the stability of the cluster number one.

Fig 13  
Fig 14

#### IV. CONCLUSIONS

We have found that the three-kink configuration which models the  $C\alpha$  backbone of the human islet amyloid polypeptide, is quite unsettled: Its low temperature limit comes endowed with six different conformational clusters. This is a marked contrast with the properties of a multi-kink configuration which models a protein that is known to possess a unique folded native state<sup>73–75</sup>. But the low temperature clustering is in accord with the intrinsically disordered character of hIAPP: The different clusters can be viewed as instantaneous snapshot conformations, between which the dynamic hIAPP swings and sways in an apparently unsettled manner which is characteristic to any intrinsically disordered protein. Furthermore, an inspection of the side-chain atoms reveals that in five of the six clusters, the hydrophobic side-chains become quite exposed to the solvent. Thus protein-solvent interactions can be expected to be present, in a manner that further enhances the dynamic character of these clusters.

But the cluster number one appears different. In this cluster the hydrophobic side-chains are less exposed. In particular the L-16 and V-32 in this cluster are positioned in a manner where they can be expected to interact attractively, in a manner that stabilizes the conformation. Indeed, this cluster has a much more localized conformational distribution than the other five clusters, and the posture comprises of two anti-parallel helices. The cluster number one is a good candidate to trigger the formation of hIAPP fibrils and amyloidosis. We propose that this cluster correspond to the intermediate  $\alpha$ -helical structures observed *e.g.* in<sup>3,12,13,16,29,30</sup>

## Acknowledgements

We thank A. Sieradzan for discussions. A.J.N. thanks A. Ramamoorthy for a communication and P. Westermark for numerous discussions on hIAPP. We acknowledge support from Region Centre Recherche d'Initiative Academique grant, Sino-French Cai Yuanpei Exchange Program (Partenariat Hubert Curien), Vetenskapsrådet, Carl Trygger's Stiftelse för vetenskaplig forskning, and Qian Ren Grant at BIT.

## References

- [1] P. Westermark, A. Andersson, G.T. Westermark, *Physiol. Rev.* **91** 795 (2011)
- [2] K. Pillay, P. Govender, *BioMed Res. Intern.* **2013** 826706 (2013)
- [3] P. Cao, P. Marek, H. Noor, V. Patsalo, L.-H. Tu, H. Wang, A. Abedini, D.P. Raleigh, *FEBS Lett.* **587** 1106 (2013)
- [4] S.E. Kahn, S. Andrikopoulos, C.B. Verchere, *Diabetes* **48** 241 (1999)
- [5] J.W. Hoppener, B. Ahren, C.J. Lips, *N. Engl. J. Med.* **343** 411 (2000)
- [6] F. Chiti, C.M. Dobson, *Annu. Rev. Biochem.* **75** 333 (2006)
- [7] L. Haataja, T. Gurlo, C.J. Huang, P.C. Butler, *Endocr. Rev.* **29** 303 (2008)
- [8] A. Lorenzo, B. Razzaboni, G.C. Weir, B.A. Yanker, *Nature* **368** 756 (1994)
- [9] N. Fox, J. Schrementi, M. Nishi, S. Ohagi, S.J. Chan, J.A. Heiserman, G.T. Westermark, A. Leckström, P. Westermark, D.F. Steiner, *FEBS Lett.* **323** 40 (1993)
- [10] J.R. Brender, S. Salamekh, A. Ramamoorthy, *Acc. Chem Res.* **45** 454 (2012)
- [11] A. Nath, A.D. Miranker, E. Rhoades, *Angew. Chem. Int. Ed. Engl.* **50** 10859 (2011)
- [12] R. Kayed, J. Bernhagen, N. Greenfield, K. Sweimeh, H. Brunner, W. Voelter, A. Kapurniotu, *J. Mol. Biol.* **287** 781 (1999)
- [13] J.D. Harper, P.T. Lansbury, *Annu. Rev. Biochem.* **66** 385 (1997)



- [14] M.O. Sumner, L.C. Serpell, *J. Mol. Biol.* **335** 1279 (2004)
- [15] S.A. Jayasinghe, R. Langen, *J. Biol. Chem.* **279** 48420 (2004)
- [16] S.A. Jayasinghe, R. Langen, *Biochemistry* **44** 12113 (2005)
- [17] D. Meetoo, P. McGovern, R. Safadi, *Br. J. Nurs.* **16** 1002 (2007)
- [18] M.R. Sawaya, S. Sambashivan, R. Nelson, *Nature* **447** 435 (2007)
- [19] S. Luca, W.M. Yau, R. Leapman, R. Tycko, *Biochemistry* **46** 13505 (2007)
- [20] R.P. Nanga, J.R. Brender, J. Xu, G. Veglia, A. Ramamoorthy, *Biochemistry* **47** 12689 (2008)
- [21] J.J.W. Wiltzius, S.A. Sievers, M.R. Sawaya, D. Cascio, D. Popov, C. Riek, D. Eisenberg, *Protein Sci.* **17** 1467 (2008)
- [22] J.J. Wiltzius, S.A. Sievers, M.R. Sawaya, D. Eisenberg, *Protein Sci.* **18** 1521 (2009)
- [23] S.M. Patil, S. Xu, S.R. Sheftic, A.T. Alexandrescu, *J. Biol. Chem.* **284** 11982 (2009)
- [24] N.F. Dupuis, C. Wu, J.E. Shea, M.T. Bowers, *J. Am. Chem. Soc.* **131** 18283 (2009)
- [25] R.P.R. Nanga, J.R. Brender, S. Vivekanandan, A. Ramamoorthy, *Biochim. Biophys. Acta: Biomembr.* **1808** 2337 (2011)
- [26] R.P. Nanga, J.R. Brender, S. Vivekanandan, A. Ramamoorthy, *Biochim. Biophys. Acta* **1808** 2337 (2011)
- [27] Y. Li, M.M. Hatmal, R. Langen, I.S. Haworth, *J. Chem. Inf. Model* **52** 2983 (2012)
- [28] S. Bedrood, Y. Li, J.M. Isas, B.G. Hedge, H. Baxa, I.S. Haworth, R. Langen, *J. Biol. Chem.* **287** 5235 (2012)
- [29] J.R. Brender, S. Salamekh, A. Ramamoorthy, *Acc. Chem Res.* **45** 454 (2012)
- [30] M. Pannuzzo, A. Raudino, D. Milardi, C. La Rosa, M. Karttunen, *Sci. Rep.* **3** 2781 (2013)

- [31] J.R. Brender, J. Krishnammoorthy, G.M.L. Messina, A. Deb, V.S. Vivekanandan, C. La Rosa, J.E. Penner-Hahn, A. Ramamoorthy, *Chem. Commun.* **49** 3339 (2013)
- [32] H.R. Patel, A.S. Pithadia, J.R. Brender, C.A. Flyrke, A. Ramamoorthy, *J. Phys. Chem. Lett.* **5** 1864 (2014)
- [33] A.K. Dunker, J.D. Lawson, C.J. Brown, R.M. Williams, P. Romero, J.S. Oh, C.J. Oldfield, A.M. Campen, C.M. Ratliff, K.W. Hipps, J. Ausio, M.S. Nissen, R. Reeves, C. Kang, C.R. Kissinger, R.W. Bailey, M.D. Griswold, W. Chiu, E.C. Garner, Z. Obradovic, *J. Mol. Graph. Mod.* **19** 26 (2001)
- [34] Y. Li, W. Xu, Y. Mu, J.Z.H. Zhang, *Journ. Chem. Phys.* **139** 055102 (2013)
- [35] W. Xu, H. Su, J.Z.H. Zhang, Y. Mu, *J. Phys. Chem.* **B116** 13991 (2012)
- [36] Q. Qiao, G.R. Bowman, X. Huang *J. Am. Chem. Soc.* **135** 16092 (2013)
- [37] C. Wu, J.-E. Shea *PLOS Comput. Biol.* **9** e1003211 (2013)
- [38] C. Miller, G.H. Zerze, J. Mittal, *J. Phys. Chem.* **B117** 16066 (2013)
- [39] G. Liang, J. Zhao, X. Yu, J. Zheng, *Biochemistry* **52** 1089 (2013)
- [40] W.M. Berhanu, U.H.E. Hansmann *PLoS ONE* **9** e97051 (2014)
- [41] W.M. Berhanu, U.H.E. Hansmann *Adv. Prot. Chem. Struct. Biol.* (in press) (2014)
- [42] D.E. Shaw, M.M. Deneroff, R.O. Dror, J.S. Kuskin, R.H. Larson, J.K. Salmon, C. Young, B. Batson, K.J. Bowers, J.C. Chao, *et al.*, *Commun. ACM* **51** 91 (2008)
- [43] K. Lindorff-Larsen, N. Trbovic, P. Maragakis, S. Piana, D.E. Shaw, *J. Am. Chem. Soc.* **134** 3787 (2012)
- [44] P. Westermarck, U. Engström, K.H. Johnson, G.T. Westermarck, C. Betsholtz, *Proc. Natl. Acad. Sci. USA* **87** 5036 (1990)
- [45] Z.L. Wang, W.M. Bennet, M.A. Ghatei, P.G. Byfield, D.M. Smith, S.R. Bloom, *Diabetes* **42** 330 (1993)
- [46] M. R. Nilsson, D. P. Raleigh, *J. Mol. Biol.* **294** 1375 (1999)

- [47] K. Tenidis, M. Waldner, J. Bernhagen, W. Fischle, M. Bergmann, M. Weber, M.-L. Merkle, W. Voelter, H. Brunner, A. Kapurniotu, *J. Mol. Biol.* **295** 1055 (2000)
- [48] C. Goldsbury, K. Goldie, J. Pellaud, J. Seelig, P. Freye, S.A. Müller, J. Kistler, G.J.S. Cooper, U. Aebi, *Journ. Struct. Biol.* **130** 352 (2000)
- [49] R. Azriel, E. Gazit, *J. Biol. Chem.* **276** 34156 (2001)
- [50] E.T.A.S. Jaikaran, C.E. Higham, L.C. Serpell, J. Zurdo, M. Gross, A. Clark, P.E. Fraser, *J. Mol. Biol.* **308** 515 (2001)
- [51] L. A. Scrocchi, Y. Chen, S. Waschuk, F. Wang, S. Cheung, A.A. Darabie, J. McLaurin, P.E. Fraser *J. Mol. Biol.* **318** 697 (2002)
- [52] Y. Mazor, S. Gilead, I. Benhar, E. Gazit, *J. Mol. Biol.* **322** 1013 (2002)
- [53] L. A. Scrocchi, K. Ha, Y. Chen, L. Wu, F. Wang, P. E. Fraser, *Journ. Struct. Biol.* **141** 218 (2003)
- [54] A. V. Kajava, U. Aebi, A. C. Steven, *J. Mol. Biol.* **348** 247 (2005)
- [55] O.V. Galzitskaya, S.O. Garbuzynskiy, M.Y. Lobanov, *Journ. Bioinf. Comput. Biol.* **4** 373 (2006)
- [56] Z. Zhang, H. Chen, L. Lai, *Bioinformatics* **23** 2218 (2007)
- [57] S.H. Shim, R. Gupta, Y.L. Ling, D.B. Strasfeld, D.P. Raleigh, M.T. Zanni, *Proc. Natl. Acad. Sci. USA* **106** 6614 (2009)
- [58] J.A. Williamson, J.P. Loria, A.D. Miranker, *J. Mol. Biol.* **393** 383 (2009)
- [59] S.M. Vaiana, R.B. Best, W.-M. Yau, W.A. Eaton, J. Hofrichter, *Biophys. J.* **97** 2948 (2009)
- [60] S.M. Cope, S. Shinde, R.B. Best, G. Ghirlanda, S.M. Vaiana, *Biophys. J.* **105** 1661 (2013)
- [61] M. Nakazato, J. Asai, M. Miyazato, S. Matsukura, K. Kangawa, H. Matsuo, *Regul. Pept.* **31** 179 (1990)

- [62] A.J. Niemi, Phys. Rev. **D67** 106004 (2003)
- [63] U.H. Danielsson, M. Lundgren, A.J. Niemi, Phys. Rev. **E82** 021910 (2010)
- [64] A.J. Niemi, [arXiv preprint arXiv:1406.7468](https://arxiv.org/abs/1406.7468) (Theoretical and Mathematical Physics, in print)
- [65] B. Widom, J. Chem. Phys. **43** 3892 (1965)
- [66] L.P. Kadanoff, Physics **2** 263 (1966)
- [67] K.G. Wilson, Phys. Rev. **B4** 3174 (1971)
- [68] M.E. Fisher, Rev. Mod. Phys. **46** 597 (1974)
- [69] M. Chernodub, S. Hu, A.J. Niemi, Phys. Rev. **E82** 011916 (2010)
- [70] N. Molkenhain, S. Hu, A.J. Niemi, Phys. Rev. Lett. **106** 078102 (2011)
- [71] S. Hu, A. Krokhotin, A.J. Niemi, X. Peng, Phys. Rev. **E83** 041907 (2011)
- [72] A. Krokhotin, A.J. Niemi, X. Peng, Phys. Rev. **E85** 031906 (2012)
- [73] A. Krokhotin, M. Lundgren, A.J. Niemi, Phys. Rev. **E86** 021923 (2012)
- [74] A. Krokhotin, M. Lundgren, A.J. Niemi, X. Peng, Journ. of Phys: Cond. Mat. **25** 325103 (2013)
- [75] A. Krokhotin, A.J. Niemi, X. Peng, J. Chem. Phys. **138** 175101 (2013)
- [76] S. Hu, Y. Jiang, A.J. Niemi, Phys. Rev. **D87** 105011 (2013)
- [77] T. Ioannidou, Y. Jiang, A.J. Niemi, Phys. Rev. **D90** 025012 (2014)
- [78] C.B. Anfinsen, Science **181** 223 (1973)
- [79] H. Frauenfelder, F. Parak, R.D. Young, Ann. Rev. Biophys. Biophys. Chem. **117** 451 (1988)
- [80] S. Hu, M. Lundgren, A.J. Niemi, Phys. Rev. **E83** 061908 (2011)
- [81] H. Schrauber, F. Eisenhaber, P. Argos, J. Mol. Biol. **230** 592 (1993)

- [82] R.L. Dunbrack Jr., M. Karplus, J. Mol. Biol. **230** 543 (1993)
- [83] S.C. Lovell, J. Word, J.S. Richardson, D.C. Richardson, Proteins **40** 389 (2000)
- [84] R.L. Dunbrack Jr., Curr. Op. Struc. Biol. **12** 431 (2002)
- [85] M.S. Shapovalov, R.L. Dunbrack Jr., Structure **19** 844 (2011)
- [86] M. Lundgren, A.J. Niemi, F. Sha, Phys. Rev. **E85** 061909 (2012)
- [87] M. Lundgren, A.J. Niemi, Phys. Rev. **E86** 021904 (2012)
- [88] A.G. Murzin, S.E. Brenner, T. Hubbard, C. Chothia, J. Mol. Biol. **247** 536 (1995)
- [89] L.H. Greene, T.E. Lewis, S. Addou, A. Cuff, T. Dallman, M. Dibley, O. Redfern, F. Pearl, R. Nambudiry, A. Reid, I. Sillitoe, C. Yeats, J.M. Thornton, C.A. Orengo, Nucl. Acids Res. **35** D291 (2007).
- [90] Y. Zhang, Curr. Opin. Struct. Biol. **19** 145 (2009)
- [91] K. Dill, S.B. Ozkan, T.R. Weikl, J.D. Chodera, V.A. Voelz, Curr. Op. Struct. Biol. **17** 342 (2007)
- [92] H.A. Scheraga, M. Khalili, A. Liwo, Ann. Rev. Phys. Chem. **58** 57 (2007)
- [93] M.A. DePristo, P.I.W. de Bakker, R.P. Shetty, T.L. Blundell, Protein Sci. **12** 2032 (2003)
- [94] S.C. Lovell, I.W. Davis, W.B. Arendall III, P.I.W. de Bakker, J.M. Word, M.G. Prisant, J.S. Richardson, D.C. Richardson, Proteins **50** 437 (2003)
- [95] P. Rotkiewicz, J. Skolnick, Journ. Comp. Chem. **29** 1460 (2008)
- [96] Y. Li, Y. Zhang, Proteins **76** 665 (2009)
- [97] G.G. Krivov, M.V. Shapovalov, R.L. Dunbrack, Jr. Proteins **77** 778 (2009)
- [98] K. Hinsen, S. Hu, G.R. Kneller, A.J. Niemi, Journ. Chem. Phys. **139** 124115 (2013)
- [99] L.D. Faddeev and L.A. Takhtajan, *Hamiltonian methods in the theory of solitons* (Springer Verlag, Berlin, 1987)

- [100] M.J. Ablowitz, B. Prinardi and A.D. Trubatch, *Discrete and continuous nonlinear Schrödinger systems* (Cambridge University Press, Cambridge, 2004)
- [101] H. Hasimoto, *J. Fluid. Mech.* **11** 477 (1972)
- [102] R.J. Glauber, *Journ. Math. Phys.* **4** 294 (1963)
- [103] A.B. Bortz, M.H. Kalos, J.L. Lebowitz, *Journ. Comput. Phys.* **17** 10 (1975)
- [104] F. Martinelli, E. Olivieri, *Comm. Math. Phys.* **161** 447 (1994)
- [105] F. Martinelli, E. Olivieri, *Comm. Math. Phys.* **161** 487 (1994)
- [106] K. Bell, R.P. May, K. Kirschner, H. Szadkowski, E. Mascher, P. Lundahl, *Eur. J. Biochem.* **190** 311 (1990)
- [107] A.M. Seddon, P. Curnow, P.J. Booth, *Biochim. Biophys. Acta* **1666** 105 (2004)
- [108] G.G. Privé, *Methods* **41** 388 (2007)
- [109] C. Michaux, N.C. Pomroy, G.G. Privé, *J. Mol. Biol.* **375** 1477 (2008)
- [110] Y. Porat, A. Stepensky, F. Naider, E. Gazit, *Biopolymers* **69** 161 (2003)
- [111] K.E. Marshall, K.L. Morris, D. Charlton, N. O'Reilly, L. Lewis, H. Walden, L.C. Serpell, *Biochemistry* **50** 2061 (2011)
- [112] A.A. Profit, V. Felsen, J. Chinwong, E.-R. E. Mojica, R.Z.B. Desamero, *Proteins* **81** 690 (2013)
- [113] V. B. Chen, W.B. Arendall III, J.J. Headd, D.A. Keedy, R.M. Immormino, G.J. Kapral, L.W. Murray, J.S. Richardson, D.C. Richardson, *Acta Cryst.* **D66** 12 (2010)
- [114] A. Krokhotin, A. Liwo, A.J. Niemi, H.A. Scheraga, *J. Chem. Phys.* **137** 035101 (2012)
- [115] M. Makowski, E. Sobolewski, C. Czaplewski, S. Oldziej, A. Liwo, H.A. Scheraga, *J. Phys. Chem.* **B112** 11385 (2008)

### Figure legends.

**Fig. 1.** Definition of Frenet frame. The tangent vector  $\mathbf{t}_i$  points from a given  $C\alpha$  atom (labeled  $i$ ) to the next  $C\alpha$  atom (labeled  $i + 1$ ). The normal vector  $\mathbf{n}_i$  is perpendicular to  $\mathbf{t}_i$  and lies in the plane defined by the  $(i - 1)^{th}$ ,  $i^{th}$  and  $(i + 1)^{th}$   $C\alpha$  atoms. The bi-normal vector  $\mathbf{b}_i$  completes the right-handed frame.

**Fig. 2.** Definitions of the backbone bond angle  $\kappa_i$  and torsion angle  $\tau_i$  in terms of the  $C\alpha$  atoms. Note the indexing.

**Fig. 3.** Interlaced NMR backbone structures of 2L86, from N-terminal (left) to C-terminal (right).

**Fig. 4.** a) The spectrum of the bond and torsion angles of 2L86 (first entry) with the convention that bond angle takes values in  $\kappa \in [0, \pi)$ . b) The spectrum of the bond and torsion angles that identifies the kink structures.

**Fig. 5.** Top: Comparison of the 3-kink bond angle (blue) with the experimental 2L86 bond angle spectrum (red). Bottom: Comparison of the 3-kink torsion angle (blue) with the experimental 2L86 torsion angle spectrum (red).

**Fig. 6.** The 3-kink solution (blue) interlaced with the 2L86 experimental structure (red).

**Fig. 7.** The black line denotes the  $C\alpha$  atom distance between the 3-kink configuration and the model 1 NMR configuration 2L86; the grey region is an estimated  $0.15 \text{ \AA}$  zero-point fluctuation distance from the 3-kink configuration. The red line denotes the B-factor Debye-Waller fluctuation distance from model 1 of 2L86. The blue-colored points denote the average  $C\alpha$  distance between the model 1 NMR structure from the average of the remaining 19 models on 2L86; the error-bars denote the maximal and minimal  $C\alpha$  distances.

**Fig. 8.** The top figure shows how the radius of gyration of the three-kink configuration evolves during heating and cooling cycle. The bottom figure shows the same for the RMSD distance from the initial configuration (the PDB structure 2L86). The red line is the average value over all configurations, and the grey zone marks the extent of the

one standard deviation from the average value. The Monte Carlo steps are displayed in multiplets of  $10^6$ .

**Fig. 9.** The distribution of all final configurations, in a run with  $\sim 1.500$  full heating and cooling cycles, classified in terms of the radius of gyration and end-to-end distance of the final configuration. Each blue dot represents a single final configuration. The six major clusters are encircled with a black ellipse; a wider grey ellipse around the clusters 3 and 5 includes some nearby scattered states. The red triangle identifies the initial configuration, the entry 1 in 2L86. Note also the presence of a cluster encircled with yellow between clusters 1 and 2.

**Fig. 10.** Superposition of all the six major clusters in Figure 9, interlaced with each other and with the PDB entry 2L86.

**Fig. 11.** Superposition of ten representative conformations (red) in each of the six clusters, as marked, together with the PDB entry 2L86 (blue).

**Fig. 12.** Conformations in Figure 9 that can be allocated side-chains with PUCLHRA (top) and SCWRL4 (bottom), with the additional condition that the distance between any two heavy atoms that are not covalently bonded to each other exceed  $1.2 \text{ \AA}$ . Note that the entire cluster encircled with yellow and located between clusters 1 and 2 in Figure 9 is present in PUCLHRA but excluded in SCWRL4.

**Fig. 13.** Hydrophobic side chains for the clusters 1-3, assigned by PULCHRA. L light blue; A dark blue; F yellow; V green; I red. In the cluster 1 the L-16 and V-32 are located very close to each other. All the other hydrophobic side-chains are exposed to the solvent.

**Fig. 14.** Hydrophobic side chains for the clusters 4-6, assigned by PULCHRA. L light blue; A dark blue; F yellow; V green; I red. All the hydrophobic side-chains are exposed to the solvent.



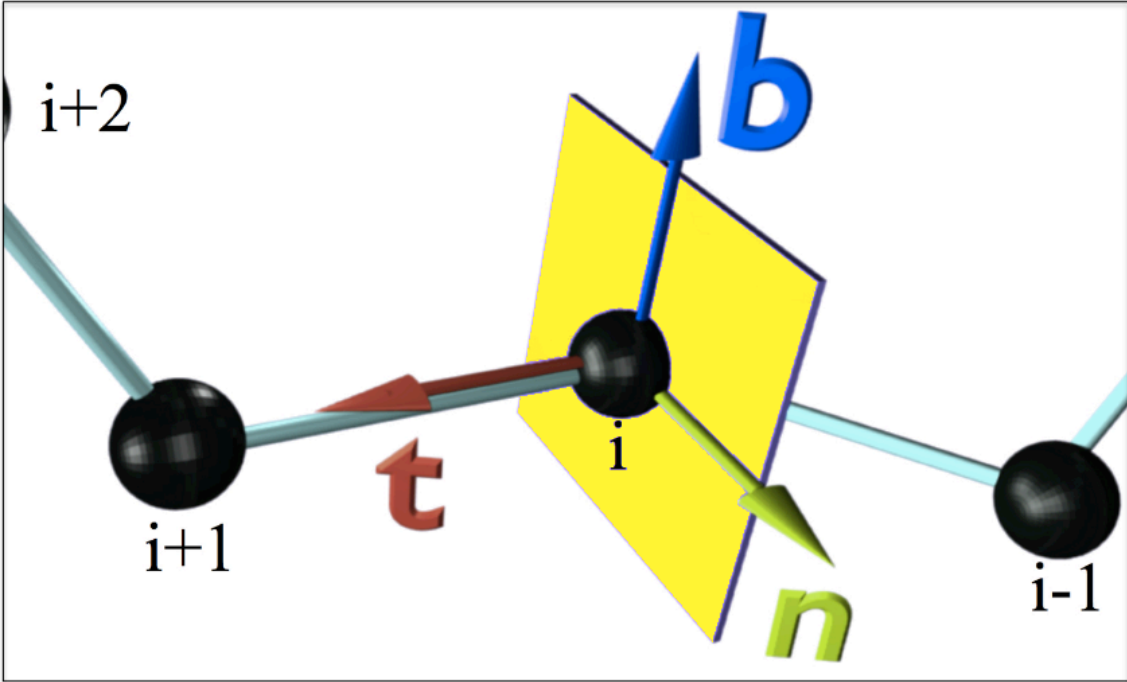


Figure 1

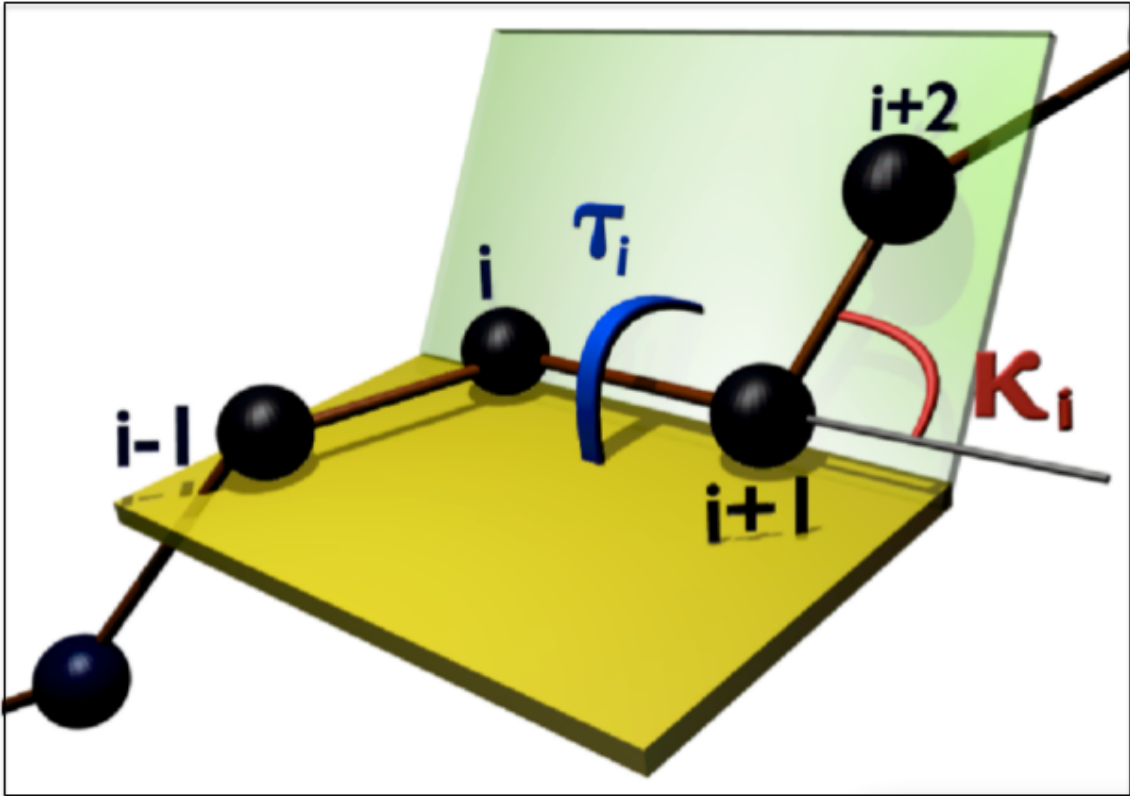


Figure 2

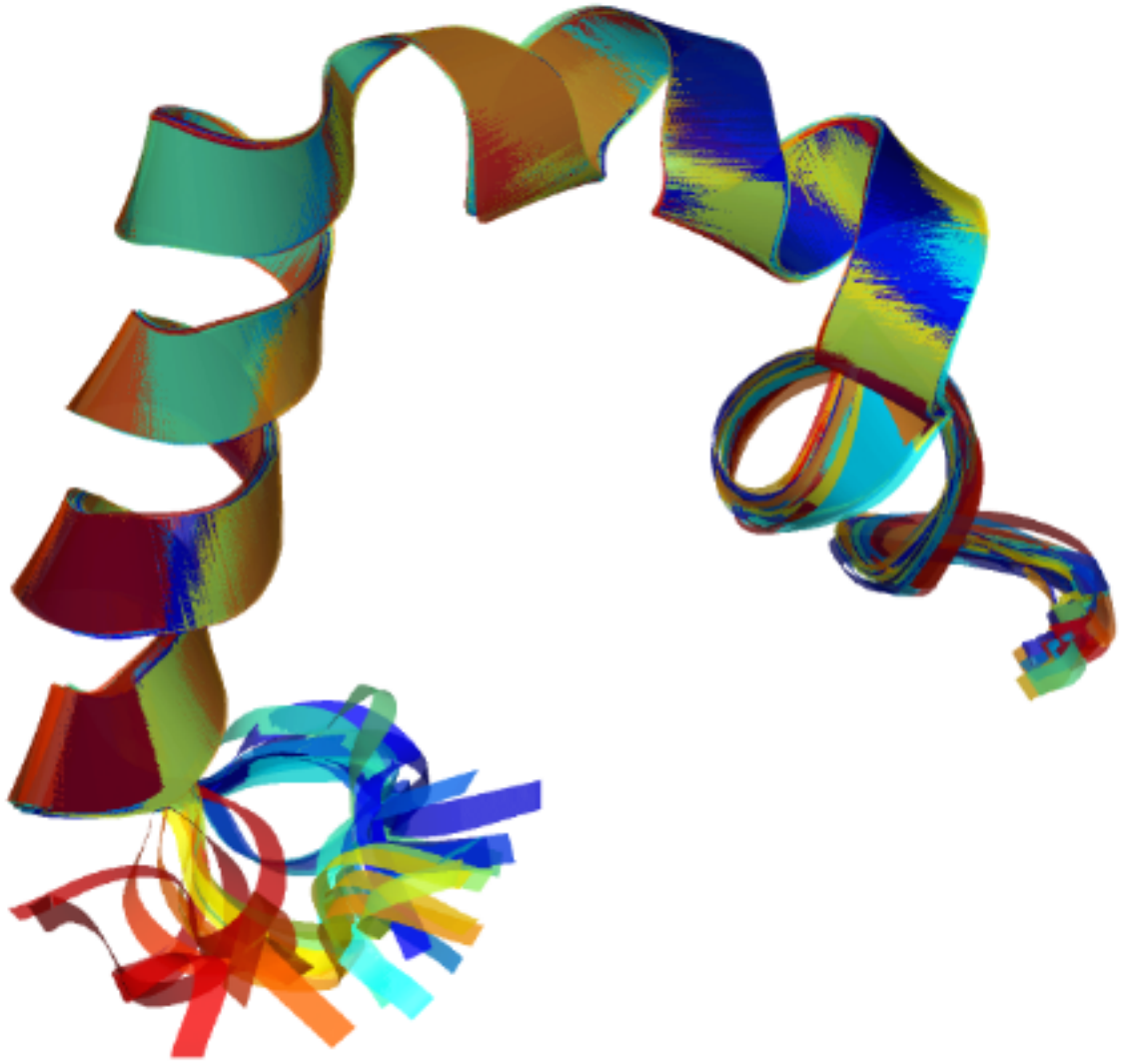


Figure 3

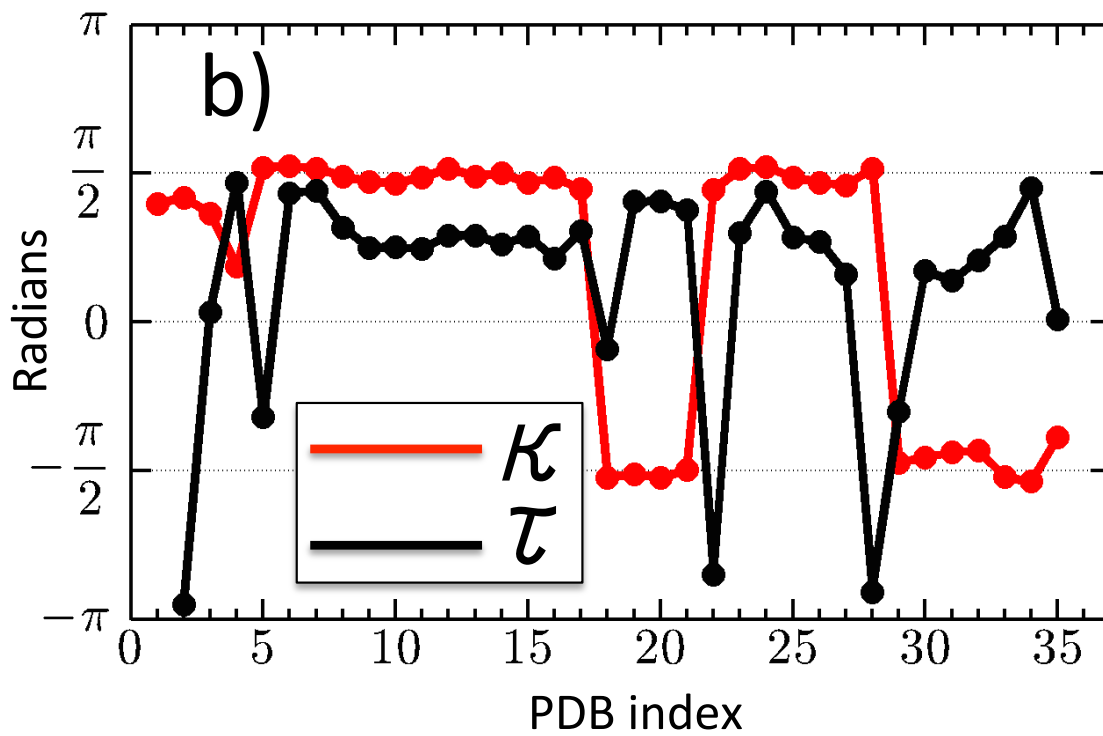
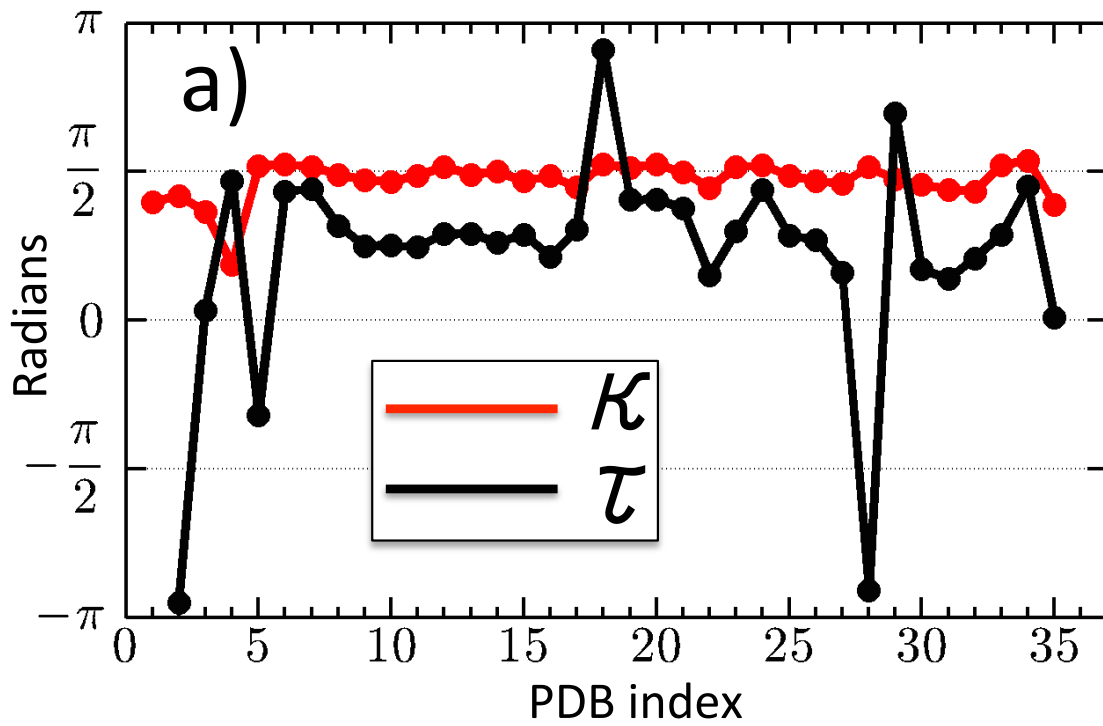


Figure 4

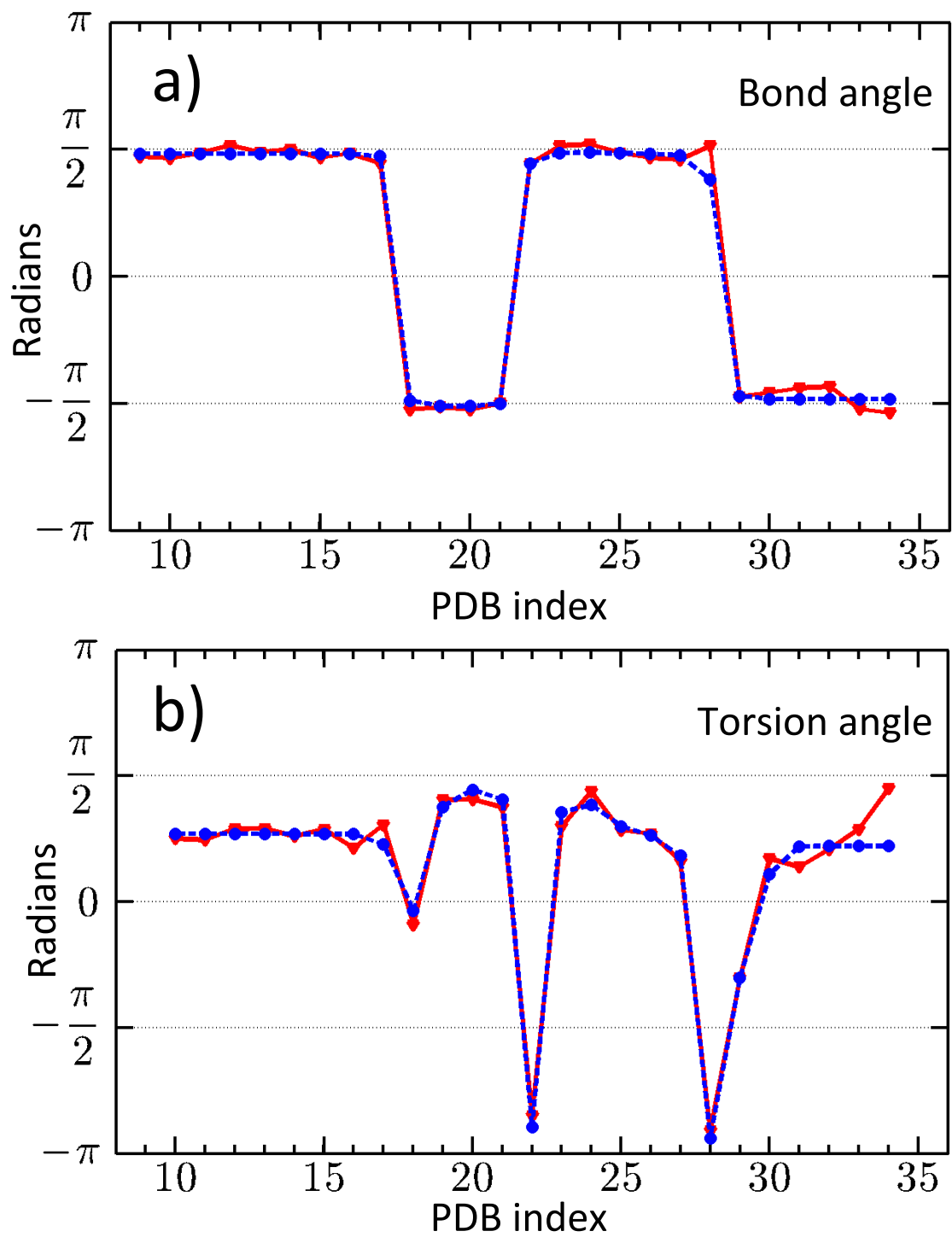


Figure 5

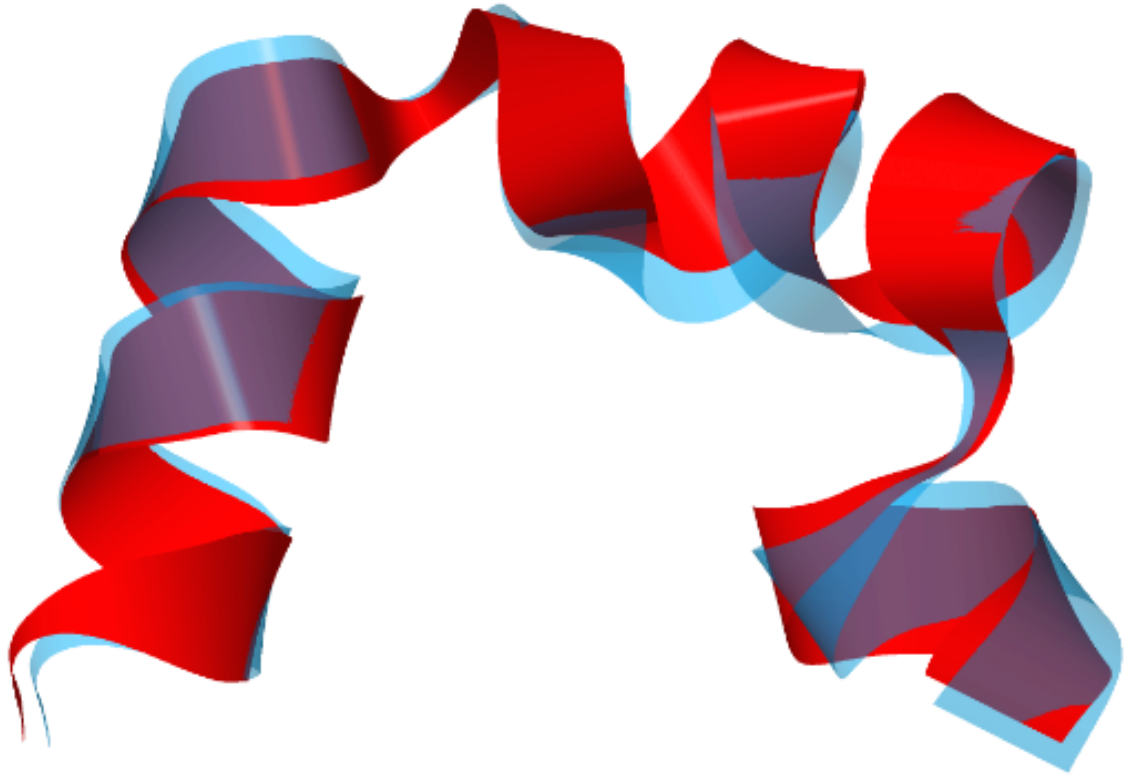


Figure 6

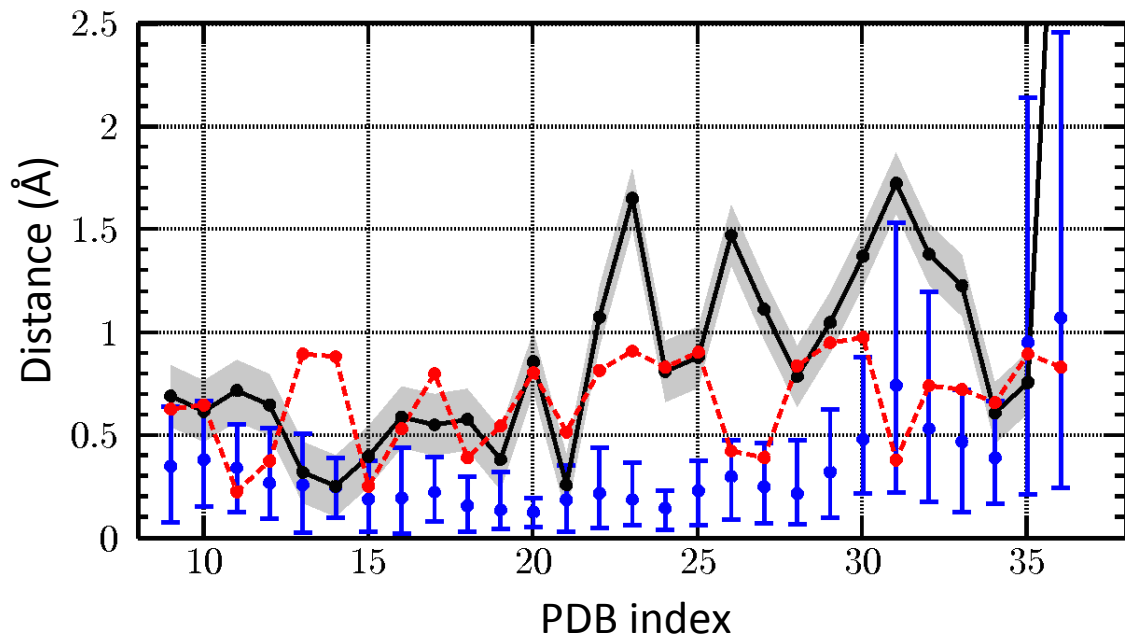


Figure 7

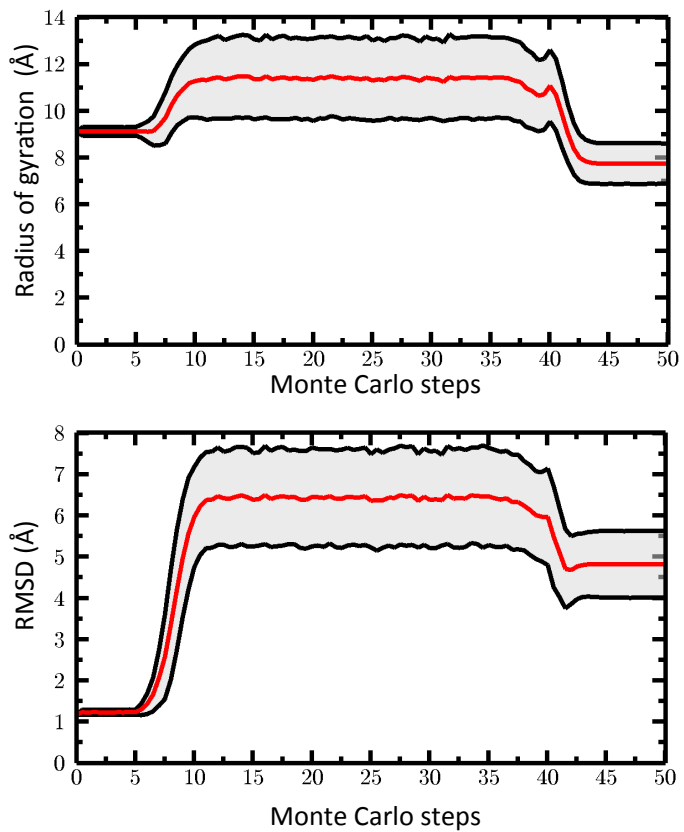


Figure 8



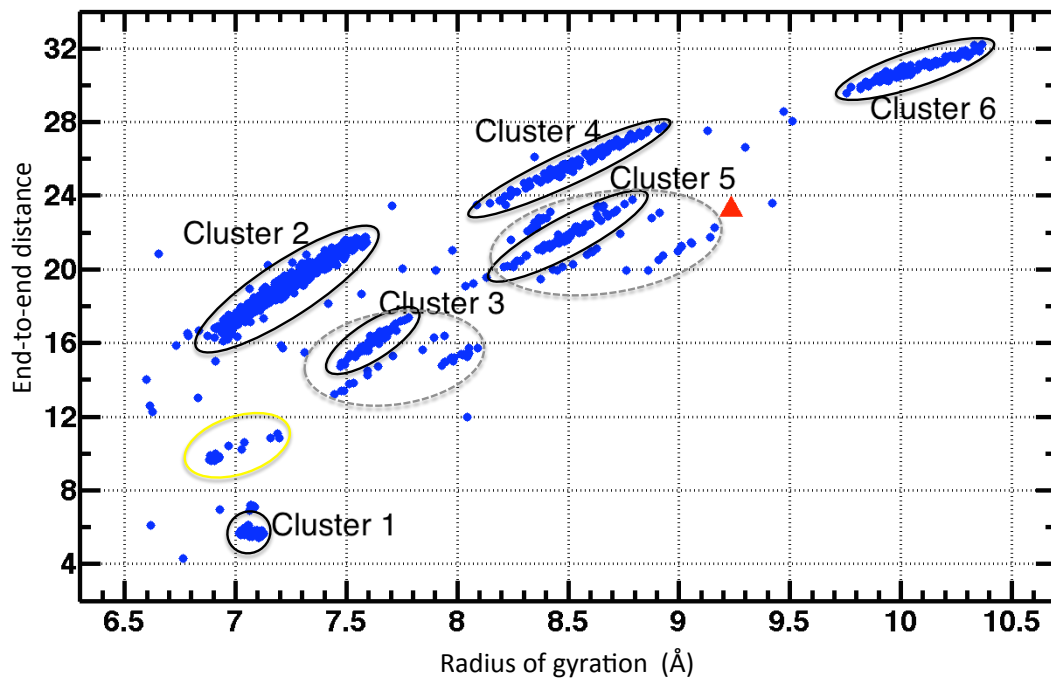


Figure 9

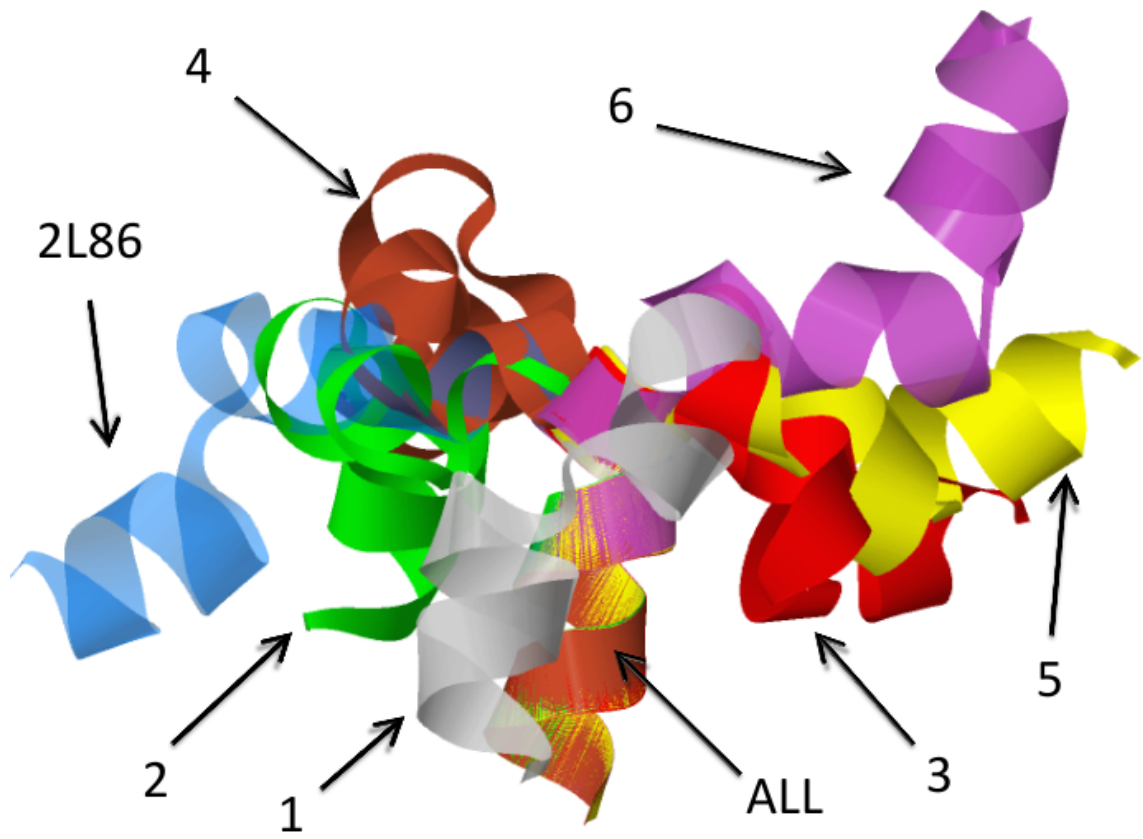


Figure 10

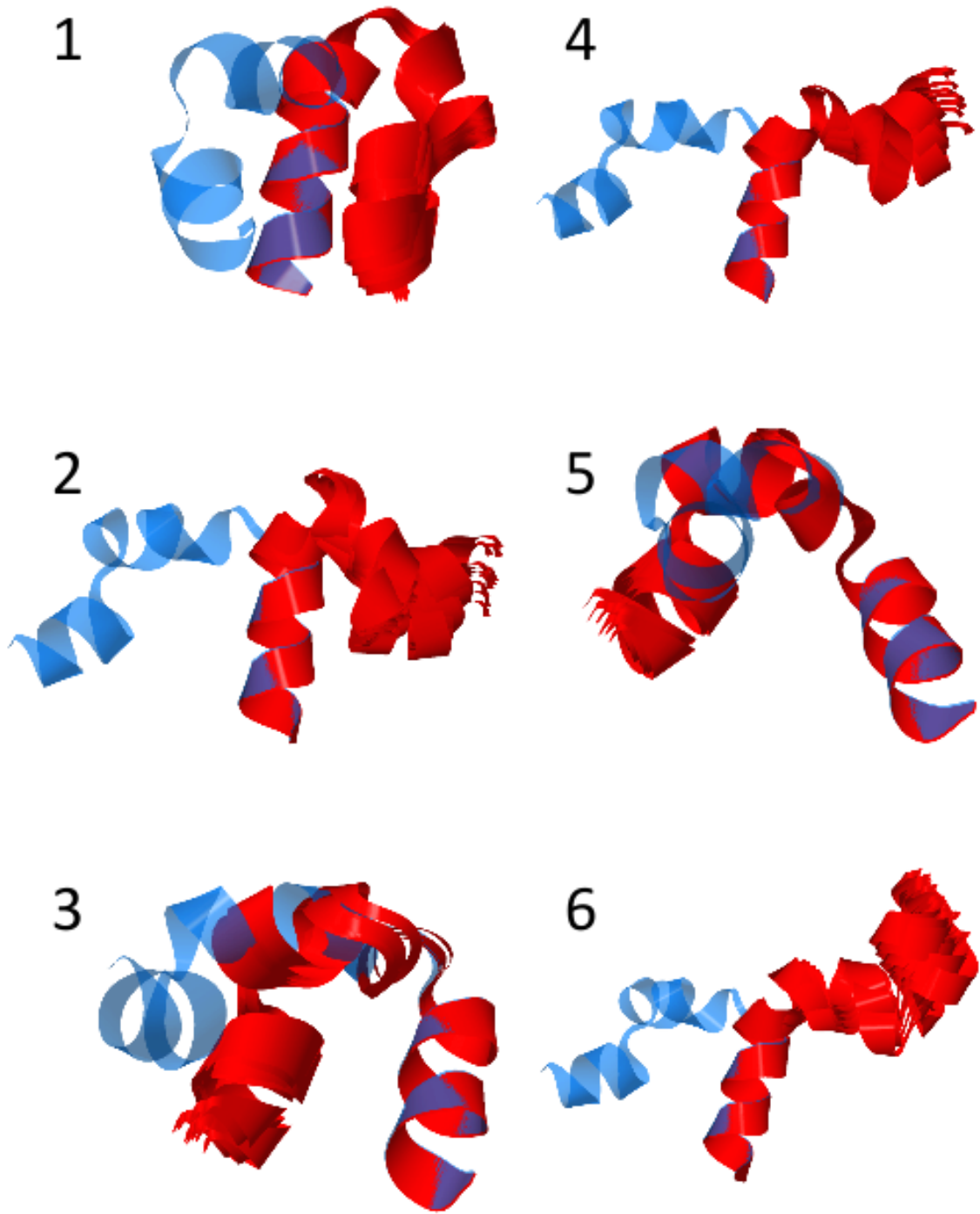


Figure 11

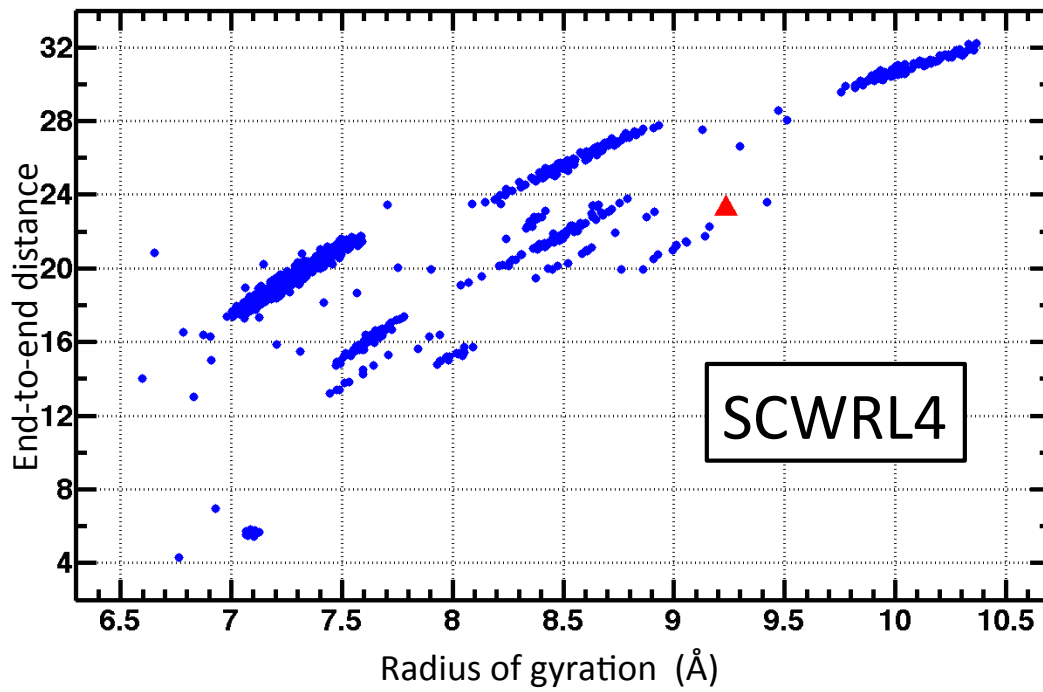
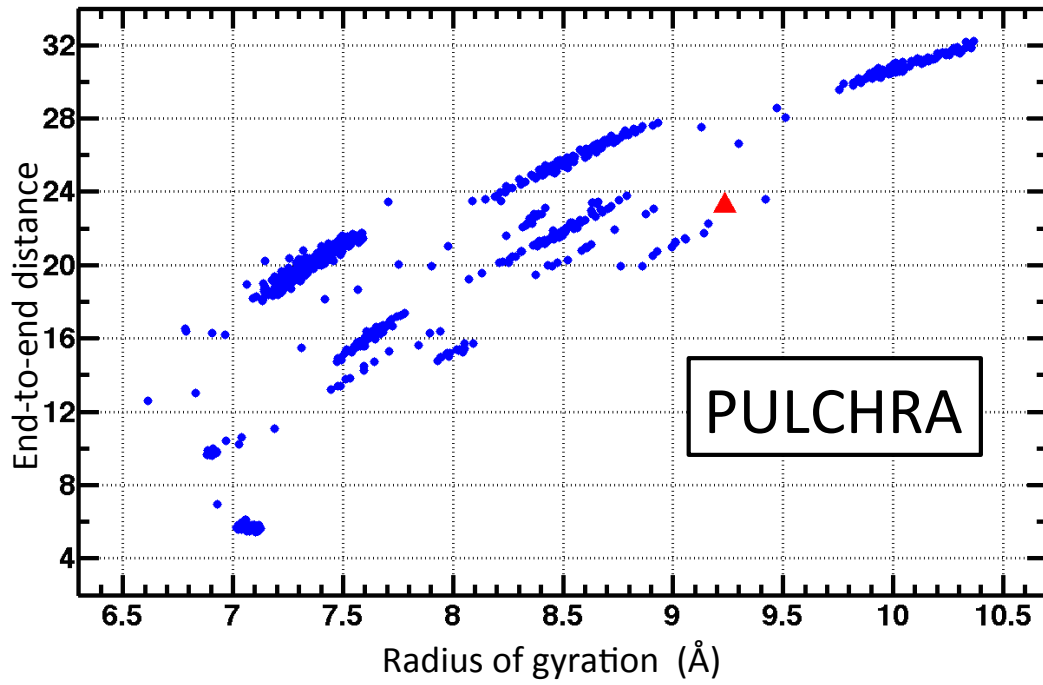
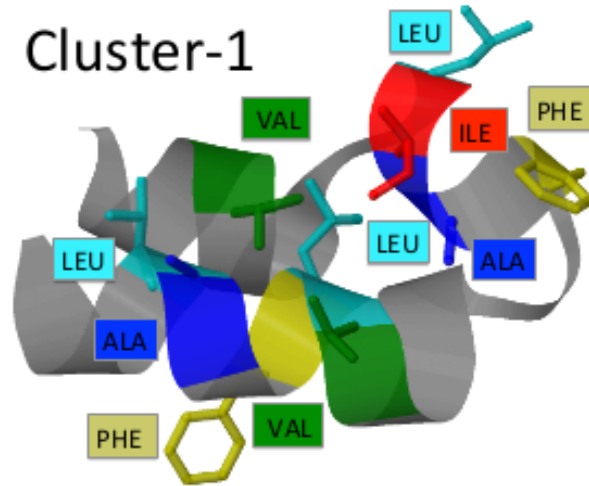
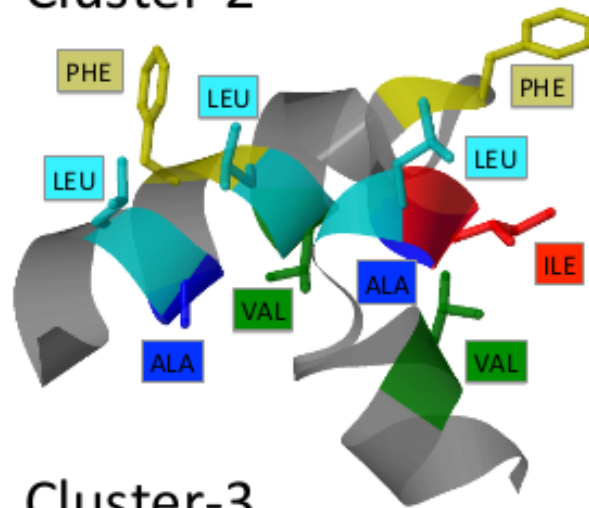


Figure 12

Cluster-1



Cluster-2



Cluster-3

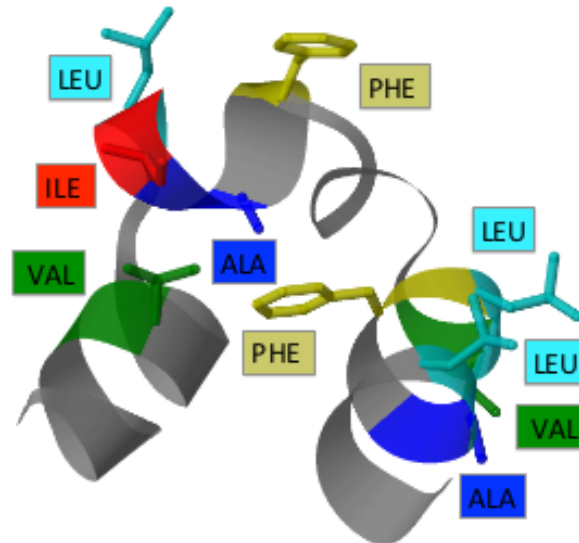
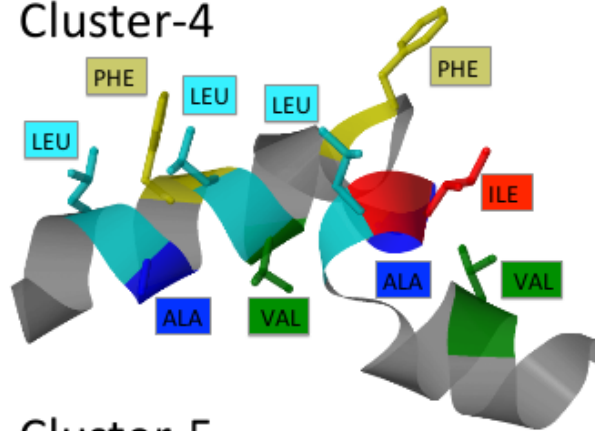
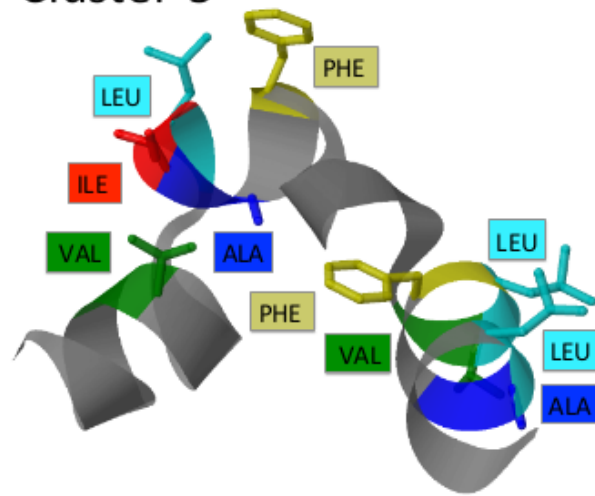


Figure 13

### Cluster-4



### Cluster-5



### Cluster-6

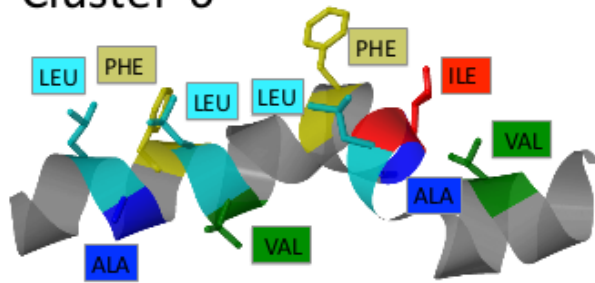


Figure 14

TABLE I: Parameter values for the three-kink configuration that describes 2L86; the soliton 1 cover the PDB segment T 9 – N 21, the soliton 2 covers the segment N 22 – A 25 and the third soliton covers the segment I 26 – T 36. The value of  $a$  is fixed to  $a = -10^{-7}$ .

soliton	$q_1$	$q_2$	$m_1$	$m_2$	$d/a$	$c/a$	$b/a$
1	9.45452	4.45398	1.52110	1.60621	$-8.1644 \cdot 10^{-2}$	$-1.4025 \cdot 10^{-3}$	-2.5688
2	2.92700	2.44082	1.66774	1.53420	$-4.8946 \cdot 10^{-1}$	$-1.0672 \cdot 10^{-3}$	- 19.4873
3	1.11956	8.08649	1.52286	1.51493	$-3.5784 \cdot 10^{-2}$	$-5.9078 \cdot 10^{-3}$	- 1.9085